JACS
JOURNAL OF THE AMERICAN CHEMICAL SOCIETY
Communication
pubs.acs.org/JACS

Allosteric Inhibitors, Crystallography, and Comparative Analysis Reveal Network of Coordinated Movement across Human Herpesvirus Proteases

Timothy M. Acker,[†] Jonathan E. Gable,[†] Markus-Frederik Bohn,[†] Priyadarshini Jaishankar,[†] Michael C. Thompson,[‡] James S. Fraser,[‡] Adam R. Renslo,[†] and Charles S. Craik*[,†]

[†]Department of Pharmaceutical Chemistry, University of California, San Francisco, California 94158, United States
[‡]Department of Bioengineering and Therapeutic Sciences, University of California, San Francisco, California 94158, United States

Supporting Information

ABSTRACT: Targeting of cryptic binding sites represents an attractive but underexplored approach to modulating protein function with small molecules. Using the dimeric protease (Pr) from Kaposi's sarcoma-associated herpesvirus (KSHV) as a model system, we sought to dissect a putative allosteric network linking a cryptic site at the dimerization interface to enzyme function. Five cryogenic X-ray structures were solved of the monomeric protease with allosteric inhibitors bound to the dimer interface site. Distinct coordinated movements captured by the allosteric inhibitors were also revealed as alternative states in room-temperature X-ray data and comparative analyses of other dimeric herpesvirus proteases. A two-step mechanism was elucidated through detailed kinetic analyses and suggests an enzyme isomerization model of inhibition. Finally, a representative allosteric inhibitor from this class was shown to be efficacious in a cellular model of viral infectivity. These studies reveal a coordinated dynamic network of atomic communication linking cryptic binding site occupancy and allosteric inactivation of KHSV Pr that can be exploited to target other members of this clinically relevant family of enzymes.

Infection by one or more of the nine herpesvirus family members is prevalent in the global population.[1] While severity of infection varies by herpesvirus subtype, these infections contribute significantly to morbidity and their effective treatment remains an important unmet clinical need. There are numerous programs aimed at developing therapeutics and elucidating new drug targets for human herpesviridae (HHV).[2] One potential therapeutic strategy for blocking the herpesvirus protease has been validated through genetic knock-out and knock-down.[3] There have been previous efforts aimed at targeting the non-canonical His-His-Ser catalytic triad that is conserved across the HHV proteases.[2]

We aimed to target a cryptic binding site that is accessed after rotameric state changes in Trp109 of Kaposi's sarcoma-associated herpesvirus protease (KSHV Pr).[4] Targeting cryptic binding sites can be challenging, since endogenous ligands for these sites are not typically available, nor is the functional effect of engaging such sites known *a priori*. Therefore, understanding how cryptic sites form, bind non-native small molecule ligands, and communicate with the rest of the protein is an active area of research, both computationally and experimentally.[5] However, there are few experimentally validated systems where cryptic pockets have been exploited for drug design.

In this study, small molecules, kinetics, and cryogenic and room-temperature X-ray crystallography were used to understand novel inhibitors that trap an inactive conformational state. Comparative analysis across the herpesvirus family identified an allosteric circuit linking distal loop regions, helix five, the cryptic binding site, and the active site. We further describe the kinetic mechanism of inhibition by these compounds, elucidating a slow, two-step mechanism of inhibition. Finally, for the first time, we demonstrate cellular efficacy with an allosteric inhibitor, suggesting that engaging this cryptic binding site is a viable strategy for inhibiting herpesvirus infectivity.

The KSHV Pr dimer (Figure 1A) is known to form via a concentration-dependent disorder-to-order transition of helix five and helix six that drive dimerization and catalytic competency. We previously described first-in-class allosteric inhibitors of KSHV that engage this dimerization interface by projecting two hydrophobic side chains from a rigid picolinamide scaffold (Figure 1A).[4] This scaffold has been shown to exhibit mixed inhibition, and similar results were obtained with compounds in this study (Table S3).[4] To more fully understand the nature of the transient, cryptic binding pocket engaged by this class of compounds, we varied the nature and connectivity of the hydrophobic side chains R^1 and R^2 that project into the cryptic binding site within KHSV Pr (Figure 1B, Tables S1 and S2).

Changing the benzylic R^1 side chain to aniline (X = CH_2 → NH) was well tolerated and enabled ready access to analogues with differentially substituted R^1 moieties. The introduction of small substituents on the aniline ring afforded analogues with IC_{50} values between 2.5 and 5.4 μM (Table S1) in a biochemical assay of KSHV Pr enzymatic activity, and similar in potency to the original inhibitors. Somewhat improved potencies, in the sub-micromolar regime, were achieved by replacing the aniline side chain with ether- or thio-ether linked aliphatic or heteroaliphatic rings at R^1.

We next explored modification of the R^2 side chain in the background of preferred alicyclic R^1 groups like cyclohexyl,

Received: April 27, 2017
Published: July 31, 2017

DOI: 10.1021/jacs.7b04030
J. Am. Chem. Soc. 2017, 139, 11650−11653

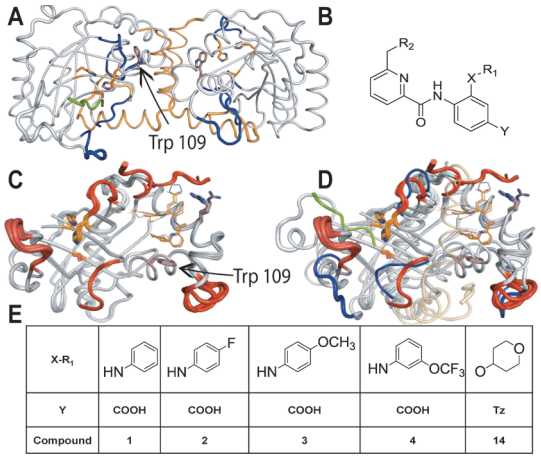

Figure 1. Binding of small molecules to the cryptic binding pocket leads to coordinated rearrangements of distal sites at the protein. (A) The KSHV protease dimer (PDB: 2PBK) is shown with the dimer interface helices in orange. Trp109 is shown in brown and blue and is located behind helix 5. The active-site residues are shown in orange, and the loop regions that adopt distinct conformations in the compound bound monomers are shown in blue. (B) The small-molecule scaffold with variable R-group regions is shown, where Y is either COOH or a tetrazole (Tz). (C) Overlay of the cryogenic co-crystal structures solved in this study (PDB codes: 5UR3, 5UVP, 5UV3, 5UTE, 5UTN). The dynamic loop regions are shown in red, scaled to their B-factors and the compounds are shown in orange. D. One monomer from the dimer structure (2PBK) is overlaid with a monomer from this study. Several loops from the monomeric structures, shown in red, are in distinct conformations from those of the dimeric structure shown in blue. (E) The R^1 groups from compounds that are co-crystallized in this study are shown (benzyl (1), 4-F-Benzyl (2), 4-OCH3-Benzyl (3), 3-OCF3-Benzyl (4), tetrahydropyran (14). Note: R^2 is cyclohexyl for each of the co-crystallized compounds. (This figure is enlarged in the Supporting Information.)

pyran, and thiopyran, and with further replacement of the carboxylate by the common acid bioisostere tetrazole. At R^2 we prepared analogues with the original cyclohexylmethyl side chain, as well as several analogues with mono- or disubstituted benzylic side chains (Table S2). These analogues exhibited a broader range of IC_{50} values ranging from 0.7 to 13.1 μM. We found that increasing hydrophobicity of the R^1 side chain improved potencies in the order pyran < thiopyran < cyclohexyl (most potent, Figure S1). By contrast, changes made to the R^2 side chain did not impact potency significantly (Table S2).

We successfully co-crystallized five new compounds (Figure 1B–D) in complex with a C-terminal Δ196 construct of the protease.[4b,6] These X-ray crystal structures have resolution ranging between 1.8 and 2.1 Å (see Supporting Information). Importantly, these structures revealed conformations of the C-terminal region and two distal loop regions, that are distinct as compared to the previously reported dimeric structure 2PBK (Figure 1B). The conformation of the oxyanion hole renders the active site incompetent for catalysis (Figure 1C).[4b] It is notable that the conformation of the oxyanion hole in these experiments differs from that of an apo-monomeric protease from the alpha-herpesvirus family.[7]

Across all molecules, the C-terminus adopts one of two conformations, both of which make critical but distinct H-bonds with the ligand. The co-crystal structure of **1** is representative of the first conformation (Figure S2A), which has two hydrogen bonding networks, one between the backbone residues (193 thru 195) and the carboxylic acid of the molecules, and one through the carboxylic acid of the small molecules and the side chain residues of T195 and R82 (Figure S2). This conformation represents a significant rearrangement of the residues as compared to the orientation in previously reported structures. In contrast, **14** adopts a distinct pattern where the C-terminal residues are directed away from the small molecule, in a similar trajectory to that of the dimeric structures (Figure S2B). These two conformations change the overall shape of the cryptic allosteric pocket and the solvent-accessible surface area is decreased in the extended conformation exemplified by **1** (Figure 2A,B).

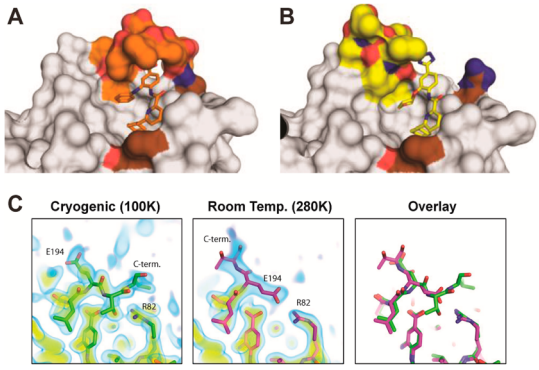

Figure 2. Distinct C-terminal conformations are identified in this study. (A) Compound **1** cryogenic co-crystal structure with the surface representation shown. The orientation of the C-terminal residues forms a well-defined pocket that encapsulates the compound. (B) Compound **14** cryogenic co-crystal structure with the surface representation shown. The orientation of the C-terminal residues leaves the anion exposed to solvent and is in a similar trajectory to that of the dimeric helices. (C) Electron density supporting temperature-dependent conformational differences between structures determined at 100 and 280 K (280 K PDB codes: 5V5D, 5V5E). The leftmost column of panel shows an electron density map and model derived from cryogenic (100 K, compound **4**) data, the middle panel shows maps and models derived from room-temperature (280 K, compound **4**) data, and the rightmost panel shows overlays of the 100 and 280 K models. The electron density maps are calculated using $2F_o-F_c$ amplitudes with model phases and are contoured at 2.5σ (yellow) or 1.0σ (blue). A nearly 180° rotation of the φ-angle of Glu194 positions the C-terminus in opposite directions in each of the two structures, leading to a slightly different set of interactions stabilizing the cryptic binding site.

To test the idea that these two conformations of the C-terminus were nearly iso-energetic, we used room-temperature data collection to avoid artifacts associated with cryo-cooling.[8] The cryogenic and 280 K structures of the protease bound to compound **4** show substantial differences where the C-terminus of the protease adopts a conformation that differs from the cryogenic structure by a 180° rotation of the φ-angle of Glu194 (Figure 2C). This structural rearrangement orients the C-terminus differently and alters polar interactions that form the cryptic binding site and places the carboxylate of E194 in close proximity to the guanidinium group of R82. The observation of these temperature-dependent conformational differences suggests that the protease retains considerable flexibility when bound to compound **4**. This additional conformation is similar to the conformation observed when bound to molecules such as **14**.

DOI: 10.1021/jacs.7b04030
J. Am. Chem. Soc. 2017, 139, 11650–11653

These structural observations led us to further explore the relationship between the dynamic regions within the co-crystal series developed here and across the ensemble of 24 published herpesvirus protease crystal structures. We calculated the root-mean-square deviations (RMSD) and root-mean-square fluctuations (RMSF) between the structures (Figure S3A,B). Notably, the loop regions identified above (residues 15−23, 80−100, and the oxyanion hole loop) show the largest RMSF across the analysis. One way to identify whether these regions exhibiting conformational variability are coordinated is with principal component analysis (PCA) of Cα distances among these similar structures (Figure S2C). The regions showing the largest RMSF are captured by principal component one, suggesting these motions are coordinated across the structures evaluated here. The combination of allosteric acting small molecules and their co-crystal structures therefore potentially inform the identification of the link between allosteric regulation of catalysis and the overall network of atomic communication across distal regions of the protein throughout the herpesvirus family.

During our elaboration of the structure−activity relationships (SAR) of compound congeners, we observed a time-dependence of inhibition with the compounds. We therefore evaluated the progress curves of the full reactions, beginning with the fractional velocity (Figure 3A). It is apparent that there is a rapid, concentration-dependent inhibition during this analysis, followed by a slow increase in inhibition over time. These observations suggest a possible two-step model of enzyme isomerization as a mechanism of inhibition. Fitting the full progress curves of the reaction for k_{obs} as a function of inhibitor concentration using the equation $P = v_s t + [(v_i - v_s)/k_{obs}](1 - \exp(-k_{obs}t))$, where P is derived from the increase in fluorescence and t is time, reveals a hyperbolic increase in k_{obs} (Figure 3B). This observation supports an enzyme isomerization model, e.g., $E \underset{k_2}{\overset{k_1[1]}{\rightleftharpoons}} EI \underset{k_4}{\overset{k_3}{\rightleftharpoons}} EI^*$, where E is the protease monomer, EI is the initial encounter complex, and EI* represents an enzyme isomerization event, with the k_{obs} values from each concentration fitting the equation $k_{obs} = k_3 + k_4[X]/(K_i + [X])$, where [X] is the inhibitor concentration.[9] The fitted K_i (note that K_i here is for the initial encounter complex) values are in good agreement with the fitted IC_{50} values (compound **1**: IC_{50} = 5.4 μM, K_i = 1.2 ± 0.7 μM, k_3 = 0.0003 ± 0.00008 s^{-1}, k_4 = 0.0001 ± 0.00007 s^{-1}; compound **14**: IC_{50} = 3.6 μM, K_i = 0.4 ± 3 μM, k_3 = 0.0003 ± 0.001 s^{-1}, k_4 = 0.0002 ± 0.001 s^{-1}, Figure 3B). We note that the error associated with these fits is relatively large due to the very slow nature of the observed kinetics and the intrinsic variability in the assay system. We therefore chose to use pre-incubation and IC_{50} as the readout in our SAR campaigns, as the modest tight-binding inhibition was challenging to fit (see Supporting Information). We also verified the reversible nature of inhibition with rapid dilution and dialysis experiments (data not shown). However, the enzyme isomerization model of inhibition fits with the observed structural rearrangements of the enzyme and the dynamic long-range coordinated networks observed in this study. When we mutated T195 to V195 (Figure 3B) in order to disrupt the hydrogen-bonding network between the side-chain residue and the carboxylic acid of the small molecules, we observe an increase in the rate for k_{obs}. This observation suggests that the isomerization can happen faster, due to less ordering of the disordered residues, a phenomenon which is known to occur when shifting equilibrium toward the monomer.

Finally, the tetrazole isostere was envisioned as a candidate for cellular studies due to the distribution of the negative charge through the nitrogenous ring and a favorable cLogD (pH 8.0) of 2.14. This compound was evaluated for efficacy in an established model of cellular re-infectivity using the iSLK.219 and SLK cells (Figure 4). The iSLK.219 cells are stably infected doxycycline (DOX) inducible KSHV+ cells (see Supporting Information). Treatment with compound **14** resulted in a dose-dependent decrease in re-infectivity as measured by flow cytometry (Figure 4A, cellular EC_{50} = 23.6 μM, 95% confidence interval 22.6−24.6 μM). The inhibition was compound specific, with a related, biochemically inactive analogue (**27**, see Supporting Information) eliciting no decrease in the re-infection readout. The potential off-target cellular effects of

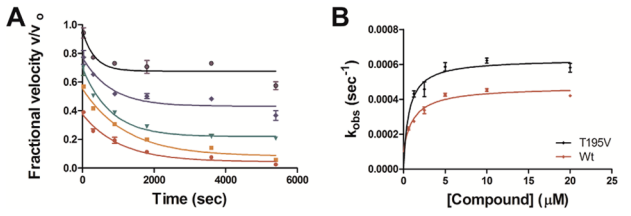

Figure 3. Compounds display slow time-dependent inhibition and two-step inhibition. (A) The fractional velocity of the reactions shows that there is a rapid, concentration-dependent inhibition followed by a slow onset to the steady state. The curves are from a two-fold dilution scheme beginning at 25 μM (red) and ending at 1.6 μM (black) of compound **14**. (B) Fitting the progress curves for k_{obs} shows a hyperbolic fit for the compounds, supporting a two-step enzyme isomerization mechanism of inhibition. The data shown are for compound **1**.

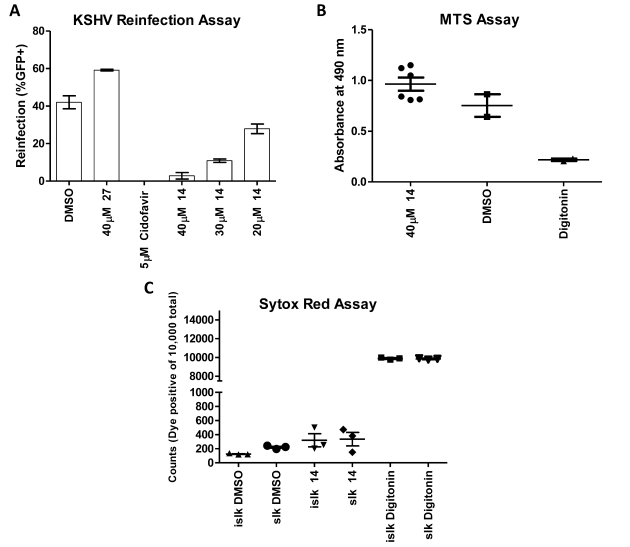

Figure 4. Cellular evaluation of a tetrazole compound **14**. (A) Compound **14** displays concentration-dependent inhibition in re-infectivity as compared to DMSO. An inactive congener shows no inhibition of re-infectivity. Cidofavir is included as a positive control. (B) Cell viability, as measured by MTS assay shows no significant differences between compound-treated and DMSO control. Digitonin served as a positive control. (C) The Sytox red assay for membrane permeability shows no significant differences between compound-treated and DMSO-treated cells for the iSLK and SLK cells.

DOI: 10.1021/jacs.7b04030
J. Am. Chem. Soc. 2017, 139, 11650−11653

compound **14** were evaluated using two methods. First, cell viability was assessed using a MTS assay (Figure 4B). There were no significant changes in metabolism or proliferation due to the presence of the analogue as compared to the DMSO controls ($p > 0.05$, one-way ANOVA, Bonferroni post-hoc analysis). Finally, the membrane permeability of the cells was assessed using the SYTOX red assay. There was no significant increase in permeability over the DMSO controls (Figure 4C, $p > 0.05$ one-way ANOVA, Bonferroni post-hoc analysis).

Exploiting cryptic binding pockets in proteins that form protein−protein interactions presents an attractive therapeutic strategy for these challenging targets. This work advances our understanding of one such example and clearly establishes a link between cryptic pocket binding and long-range atomic communication. The opportunity to maintain the bound state via slow off rates at cryptic sites near protein interfaces otherwise requiring high surface area of binding holds the potential to allow small-molecule drug-like compounds to make further progress in modulating these challenging targets.

This study describes various cryogenic and room-temperature co-crystal structures that, through comparative analysis, identify the distal regions most likely associated with the allosteric pathway of atomic communication across the herpesvirus family of proteases. Our analysis further suggests that the cryptic binding pocket shape is not rigid across the compound series assessed here; indeed, temperature dependence suggests residual plasticity of distinct H-bonding patterns between the C-terminus and ligand can be further optimized to create more potent molecules. Both this plasticity and the analysis of the ensemble of all related proteases are consistent with the two-step mechanism of inhibition and induced fit type kinetics that we observe.

Finally, we establish cellular efficacy with this class of small molecules, which supports the idea that allosteric targeting of the herpesvirus proteases could be a tractable therapeutic strategy. The observed efficacy with the compounds represents a significant step forward in the pursuit of novel therapeutic strategies against human herpesviruses. We believe that the link between protein−protein interaction and the resulting allosteric networks that the herpesvirus family of proteases relies on presents an opportunity to target other viruses in a similar manner.

■ ASSOCIATED CONTENT

Supporting Information

The Supporting Information is available free of charge on the ACS Publications website at DOI: 10.1021/jacs.7b04030.

Experimental details and analytical and characterization data, including Tables S1−S3 and Figures S1−S7 (PDF)

■ AUTHOR INFORMATION

Corresponding Author

*charles.craik@ucsf.edu

ORCID

Adam R. Renslo: 0000-0002-1240-2846

Charles S. Craik: 0000-0001-7704-9185

Notes

The authors declare no competing financial interest.

■ ACKNOWLEDGMENTS

We would like to acknowledge Christopher A. Waddling for helpful discussions, as well as Andrew Van Benschoten for assistance with room-temperature data collection. We would also like to acknowledge the National Institutes of Health for funding (R01-AI090592 to C.S.C., 1F32GM111012 to T.M.A.). J.E.G. was supported by NIH Structural Biology Training Grant GM008284 and the National Science Foundation Graduate Research Fellowship Program (1144247).

■ REFERENCES

(1) *Human Herpesviruses: Biology, Therapy, and Immunoprophylaxis*; Arvin, A, Gabriella, C.-F., Mocarski, E, Moore, P. S., Roizman, B., Whitely, R., Yamanishi, K., Eds.; Cambridge University Press: Cambridge, 2007; https://www.ncbi.nlm.nih.gov/books/NBK47376/.

(2) Gable, J. E.; Acker, T. M.; Craik, C. S. *Chem. Rev.* **2014**, *114* (22), 11382−11412.

(3) Preston, V. G.; Coates, J. A. V.; Rixon, F. J. *J. Virol.* **1983**, *45* (3), 1056−1064.

(4) (a) Shahian, T.; Lee, G. M.; Lazic, A.; Arnold, L. A.; Velusamy, P.; Roels, C. M.; Guy, R. K.; Craik, C. S. *Nat. Chem. Biol.* **2009**, *5* (9), 640−646. (b) Lee, G. M.; Shahian, T.; Baharuddin, A.; Gable, J. E.; Craik, C. S. J. *J. Mol. Biol.* **2011**, *411* (5), 999−1016.

(5) Cimermancic, P.; Weinkam, P.; Rettenmaier, T. J.; Bichmann, L.; Keedy, D. A.; Woldeyes, R. A.; Schneidman-Duhovny, D.; Demerdash, O. N.; Mitchell, J. C.; Wells, J. A.; Fraser, J. S.; Sali, A. J. *J. Mol. Biol.* **2016**, *428* (4), 709−719.

(6) Gable, J. E.; Lee, G. M.; Jaishankar, P.; Hearn, B. R.; Waddling, C. A.; Renslo, A. R.; Craik, C. S. *Biochemistry* **2014**, *53* (28), 4648−4660.

(7) Zuehlsdorf, M.; Werten, S.; Klupp, B. G.; Palm, G. J.; Mettenleiter, T. C.; Hinrichs, W. *PLoS Pathog.* **2015**, *11*, e1005045.

(8) Fraser, J. S.; van den Bedem, H.; Samelson, A. J.; Lang, P. T.; Holton, J. M.; Echols, N.; Alber, T. *Proc. Natl. Acad. Sci. U. S. A.* **2011**, *108* (39), 16247−16252.

(9) Morrison, J. F.; Walsh, C. T. *Adv. Enzymol. Relat. Areas Mol. Biol.* **2006**, *61*, 201−301.

DOI: 10.1021/jacs.7b04030
J. Am. Chem. Soc. 2017, 139, 11650−11653